

Using spin bias to manipulate and measure quantum spin in quantum dots

Hai-Zhou Lu and Shun-Qing Shen

*Department of Physics, and Centre of Theoretical and Computational Physics,
The University of Hong Kong, Pokfulam Road, Hong Kong, China**

(Dated: November 28, 2018)

A double-quantum-dot coupled to electrodes with spin-dependent splitting of chemical potentials (spin bias) is investigated theoretically by means of the Green's functions formalism. By applying a large spin bias, the quantum spin in a quantum dot (the dot 1) can be manipulated in a fully electrical manner. To noninvasively monitor the manipulation of the quantum spin in the dot 1, it is proposed that the second quantum dot (the dot 2) is weakly coupled to the dot 1. In the presence of the exchange interaction between the two dots, the polarized spin in the dot 1 behaves like an effective magnetic field and weakly polarizes the spin in the nearby quantum dot 2. By applying a very small spin bias to the dot 2, the spin-dependent transport through the dot 2 can be probed, allowing the spin polarization in the dot 1 to be identified nondestructively. These two steps form a complete scheme to manipulate a trapped spin while permitting this manipulation to be monitored in the double-dot system using pure electric approaches.

PACS numbers: 85.75.-d, 73.21.La, 72.25.-b, 72.25.Hg

I. INTRODUCTION

Manipulation and measurement of single electron spin in a quantum dot is the basis towards scalable spin-based quantum information processing.¹ Rapid progresses of the charging sensing technique^{2,3} make it possible to control the number of electrons inside quantum dots precisely down to few electrons,⁴ allowing an individual electron spin to be manipulated^{5,6} and read-out^{7,8} with help of either stationary or precisely controlled oscillating electromagnetic field. The significance of the charging sensing technique is that it makes use of a nearby quantum point contact to noninvasively measure the electron number in the quantum dot, which avoids destructing the electron occupation in the quantum dot by direct transport measurement. From the point of view of spin-based quantum information processing, it would be highly desirable to design a similar device with integrated abilities to manipulate a trapped single spin while permitting the manipulation to be read out nondestructively in quantum dot. Most importantly, a pure electric approach (in the absence of magnetic or optical field) is particularly appealing because it will contribute to large-scale integration.

A possible direction of effort is spin injection technique, i.e. generating a nonequilibrium spin accumulation in nonmagnetic (paramagnetic) materials, which could induce a spin-dependent splitting of chemical potentials or spin bias in the injected materials. The spin injection has been achieved by using various of electric and optical approaches. One of the popular ones is to inject spins directly from ferromagnetic to nonmagnetic materials.⁹ The materials and geometries used in this method include metals,^{10,11,12} metal/barrier/semiconductors,^{13,14,15} and ferromagnetic/normal semiconductors.^{16,17} In the last few years, spin injection has also been realized by means of the spin Hall effect,^{18,19} and incidence of linearly or circularly polarized light into 2-dimensional electron gas

with spin-orbital coupling.^{20,21,22} Notice that many of the intensively investigated spin-injected nonmagnetic materials are also widely used to fabricate electrodes probing semiconductor²³ and single-molecule quantum dots.²⁴ Therefore, it is interesting to investigate polarization and detection of electron spin in quantum dot systems using electrodes with spin bias.

Experimentally, spin injection into all-semiconductor quantum dots has been reported, from (Ga,Mn)As to InAs QDs²⁵, and from BeMnZnSe to a single CdSe/ZnSe QD, both combined with spin-LED to detect spin polarization. Besides, several theoretical works began to address the transport through mesoscopic systems in the presence of spin-splitting of chemical potentials.^{26,27,28,29,30,31}

Motivated by these experimental and theoretical progresses, we propose a scheme to realize the control and detection of quantum spin in semiconductor quantum dot by using spin bias or spin current. Our setup consists of a double-quantum-dot system connected to electrodes as shown in Fig. 1. It is worth stressing that as the spin injection techniques in various means are still under extensive investigations and progresses, in the present work, we focus only on the physical consequences of spin bias or spin current, and ignore the approaches to generate the spin bias. To generate a quantum spin state, we apply a spin bias on the electrode coupling the quantum dot 1 (Fig. 1(a)). Suitable parameters will be chosen to maintain a single electron (or an odd number of electrons) in the dot 1. The spin bias V_1 induces a splitting between the Fermi levels $\mu_{1\uparrow/\downarrow}$ for spin up \uparrow (down \downarrow) electrons in the lead L1. The occupation of electron with specific spin orientation is energetically determined by the relative location between the dot level ϵ_1 , on-site repulsion U_1 , and the Fermi levels $\mu_{1\uparrow/\downarrow}$. As a result, the quantum spin in the dot 1 can be manipulated in a fully electrical manner (Fig. 1(a)). To detect the state of electron spin we apply a smaller spin bias V_2 to the dot 2, which cou-

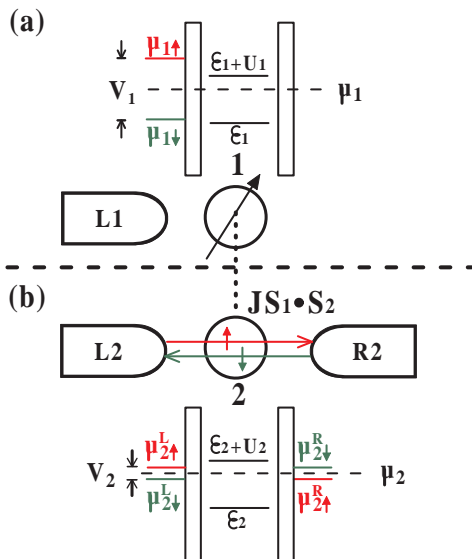


FIG. 1: (Color online) Schematic illustration of our double-dot system, in which each dot is attached to its own electrodes with spin-dependent splitting of chemical potentials (spin biases). (a) A large spin bias V_1 is applied to manipulate the quantum spin in the dot 1. The energy zero point is set at $\epsilon_1 + U_1/2$. The spin bias V_1 induces a splitting of the Fermi levels for \uparrow and \downarrow electrons in the lead L1 so that $\mu_{1\uparrow/\downarrow} = \mu_1 \pm V_1/2$, where μ_1 is the middle point of the Fermi levels. (b) Due to the exchange interaction between the two dots, the polarized spin in the dot 1 behaves like an effective magnetic field and weakly polarizes the spin in the dot 2. A very small spin bias V_2 is applied to the dot 2 to probe its spin-dependent transport, allowing the spin polarization in the dot 1 to be read out nondestructively. μ_2 is the equilibrium Fermi level for both leads L2 and R2. The spin bias V_2 induces a splitting of the Fermi levels for $\uparrow(\downarrow)$ electrons in the leads of dot 2, so that $\mu_{2\uparrow/\downarrow}^L = \mu_2 \pm V_2/2$ and $\mu_{2\uparrow/\downarrow}^R = \mu_2 \mp V_2/2$.

ples to the dot 1 (Fig. 1 (b)). In the presence of exchange interaction between the two dots, the polarized spin in the dot 1 behaves like an effective magnetic field to the dot 2. As a result it will induce a charge current when a spin bias is applied or a spin current flows through the dot 2, allowing the spin polarization in the dot 1 to be identified nondestructively (Fig. 1 (b)). These two steps form a complete scheme of manipulating and measuring the quantum spin state of a trapped electron in the double-dot system using purely electric means.

The present paper is organized as follows. In Sec. II, the manipulation of quantum spin in the dot 1 is addressed. The quantum spin in the dot can be controlled very well by the spin bias. The stability diagrams of electron number and spin polarization in the dot 1 are presented. In Sec. III, the measurement to the spin polarization in the dot 1 using the spin-dependent transport through the dot 2 is discussed. A detailed analytical calculation and numerical results are presented. We focus on the charge current induced by the spin bias or spin conductance, which can be measured experimentally to

determine the spin state in the coupled quantum dots. In Sec. IV, as a summary, we compare our system (or named spin sensing technique) with the charge sensing technique. At last the detailed calculations of spin conductance and Green's functions are attached in two appendices for reference.

II. MANIPULATION OF QUANTUM SPIN BY MEANS OF SPIN BIAS

As shown in Fig. 1, our model includes two quantum dots which are coupled weakly. The dot 1 is designed to host the quantum spin to be manipulated, and the dot 2 is for measurement of the electron spin in the dot 1. We first focus on the manipulation of electron spin in the dot 1 by using the spin bias.

Without loss of generality, we consider only one energy level in the dot 1. Besides, to retain electrons in the dot 1, we consider only one reservoir to avoid electron transport in the usual two-reservoir case. As shown in Fig. 1(a), the dot level ϵ_1 is spin-degenerate. When we apply a spin bias V_1 in the reservoir, the Fermi levels of the reservoir are spin-resolved (denoted as $\mu_{1\uparrow}$ and $\mu_{1\downarrow}$). When the dot 1 is coupled to its reservoir, the electron number inside it at low temperatures will be determined by the relative location between the dot level ϵ_1 and the Fermi levels of the reservoir. In the absence of spin-dependent splitting of chemical potentials ($\mu_{1\uparrow} = \mu_{1\downarrow}$), it is known that the dot will be filled or empty when the Fermi levels are well above or below the dot level. Similarly, in the presence of the spin-resolved Fermi levels, the filling of $\uparrow(\downarrow)$ electron in the dot 1 is determined independently by the relative location between ϵ_1 and $\mu_{1\uparrow}(\mu_{1\downarrow})$. The simplest situation is that when $\mu_{1\downarrow} < \epsilon_1 < \mu_{1\uparrow}$, only \uparrow electron is energetically allowed to stay in the dot, therefore the electron spin in the dot is \uparrow polarized. General speaking, the spin polarization of the electron in the dot can be controlled by the spin bias. When considering the on-site Coulomb repulsion, detailed calculations are required and presented in the following subsections.

A. The model and spin bias

The dot 1 is described by the Anderson model³²

$$H_1 = \sum_{\sigma} \epsilon_1 n_{1\sigma} + U_1 n_{1\uparrow} n_{1\downarrow} + \sum_{k,\sigma} \epsilon_{k\sigma} c_{k\sigma}^{\dagger} c_{k\sigma} + \sum_{k,\sigma} (V_{k\sigma} c_{k\sigma}^{\dagger} d_{1\sigma} + h.c.), \quad (1)$$

where $d_{1\sigma}^{\dagger}(d_{1\sigma})$ represents the creation (annihilation) operator for the discrete state with the energy ϵ_1 and spin $\sigma(\in\{\uparrow,\downarrow\})$ in the dot 1, the number operator $n_{1\sigma} = d_{1\sigma}^{\dagger} d_{1\sigma}$, and U_1 is the intra-dot Coulomb repulsion. $c_{k\sigma}^{\dagger}(c_{k\sigma})$ is the creation (annihilation) operator for

a continuous state in the lead (reservoir) L1 with energy $\epsilon_{k\sigma}$ and spin σ . The tunneling matrix element $V_{k\sigma}$ is assumed to be independent of k in the following calculations. In Eq. (1), we have ignored the dot 2 and the spin correlation between the dots 1 and 2, which is used to noninvasively detect the spin polarization in the dot 1. The validity of this approximation will be discussed in Sec. III B.

The energy zero point is set at $\epsilon_1 + U_1/2$. As shown in Fig. 1, we denote by $\mu_{1\sigma}$ the Fermi level for σ electrons in the lead L1. The spin bias V_1 is introduced phenomenologically as a splitting of the Fermi levels for spin \uparrow and \downarrow electrons in the lead L1 so that

$$\begin{aligned}\mu_{1\uparrow} &= \mu_1 + V_1/2, \\ \mu_{1\downarrow} &= \mu_1 - V_1/2,\end{aligned}$$

where μ_1 is the middle point of the Fermi levels

$$\mu_1 = \frac{1}{2}(\mu_{1\uparrow} + \mu_{1\downarrow}),$$

which can be tuned with respect to ϵ_1 by gate voltage.

B. Spin Polarization and Green's Function Technique

In order to determine the optimal parameters to polarize a single spin, we calculate the polarization of the electron spin $\langle s_1^z \rangle = (\langle n_{1\uparrow} \rangle - \langle n_{1\downarrow} \rangle)/2$ and the total electron number $\langle n_1 \rangle = \langle n_{1\uparrow} \rangle + \langle n_{1\downarrow} \rangle$ in the dot 1 as functions of the spin bias V_1 and the middle point μ_1 of the Fermi level. The formula for the σ component of particle number $\langle n_{1\sigma} \rangle$ can be expressed in terms of the lesser Green's function^{33,34}

$$\langle n_{1\sigma} \rangle = -i \int \frac{d\omega}{2\pi} G_{1\sigma}^<(\omega),$$

where

$$G_{1\sigma}^< = G_{1\sigma}^r \Sigma_{1\sigma}^< [G_{1\sigma}^r]^\dagger, \quad \Sigma_{1\sigma}^< = i\Gamma_1 f_{1\sigma},$$

where $\mathbf{G}_{1\sigma}^r(\omega)$ is the retarded Green's functions defined as the Fourier transform of $G_{1\sigma}^r(t) = -i\theta(t)\langle\{d_{1\sigma}(t), d_{1\sigma}^\dagger\}\rangle$, $d_{1\sigma}(t) = e^{iH_1 t} d_{1\sigma} e^{-iH_1 t}$. $\Gamma_1 = \sum_k 2\pi |V_{k\sigma}|^2 2\pi\delta(\omega - \epsilon_{k\sigma})$ is the broadening of the quantum dot level ϵ_1 , due to its coupling to the lead L1 for \uparrow or \downarrow electrons. Γ_1 is assumed to be independent of σ , since we are not addressing a ferromagnetic electrode. $f_{1\sigma}$ is the Fermi-Dirac distribution of σ electrons in the lead,

$$f_{1\sigma}(\omega) = \frac{1}{e^{(\omega - \mu_{1\sigma})/k_B T} + 1},$$

where T is the temperature and k_B the Boltzmann constant. Up to the second-order of Hartree-Fock approximation, the retarded Green's function of the dot 1 is given by³³

$$G_{1\sigma}^r = \frac{1 - \langle n_{1\bar{\sigma}} \rangle}{\omega - \epsilon_1 + \frac{i}{2}\Gamma_1} + \frac{\langle n_{1\bar{\sigma}} \rangle}{\omega - \epsilon_1 - U_1 + \frac{i}{2}\Gamma_1}.$$

Here we do not consider the Kondo effect in the dot because it is usually suppressed due to the large spin bias V_1 .

C. Numerical results

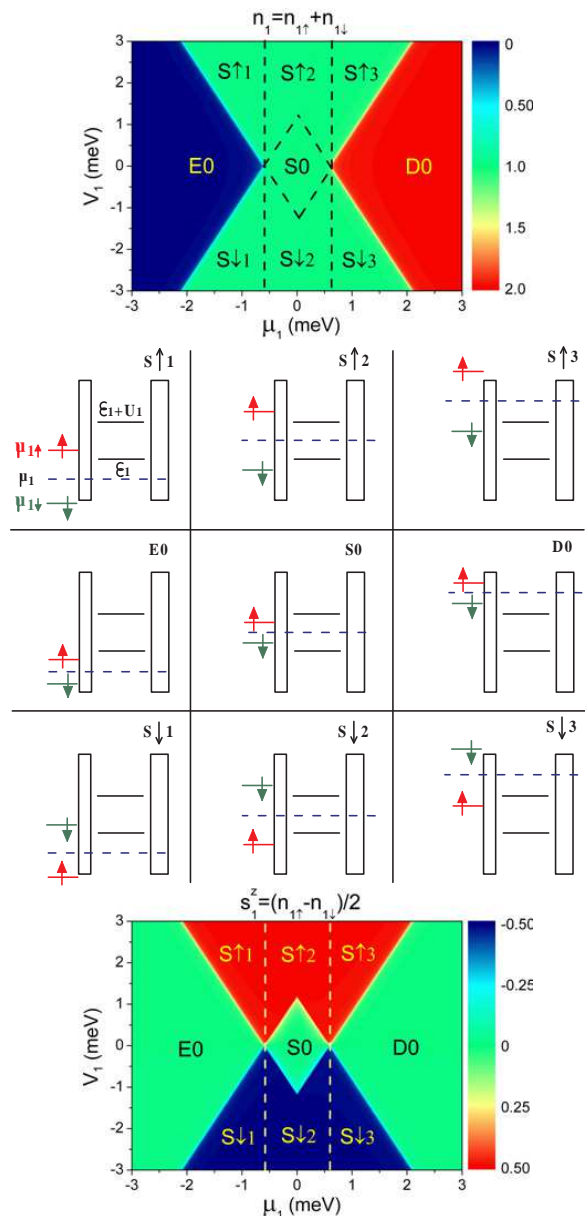


FIG. 2: (Color online) The total electron number $\langle n_1 \rangle$ (top panel) and spin polarization $\langle s_1^z \rangle$ (bottom panel) diagrams as functions of the spin bias V_1 and the Fermi level middle point μ_1 . The diagrams can be divided into 9 configurations, schematically shown in the middle panel, starting from 3 unpolarized states E0, S0, and D0 with the electron number $n_1 = 0, 1, 2$ respectively. Where E=empty, S=singly-occupied, D=doubly-occupied, and 0, \uparrow , and \downarrow represent unpolarized and two polarized states.

The electron number $\langle n_1 \rangle$ and spin-polarization $\langle s_1^z \rangle$ diagrams are shown in Fig. 2 as functions of the pure spin bias V_1 and the Fermi level middle point μ_1 . In the calculations, we choose a set of typical parameters $k_B T = 0.004$ meV, $U_1 = 1.2$ meV, $\Gamma_1 = 0.0375$ meV, in accordance with the experiment.³⁵ $\epsilon_1 = -0.6$ meV to assure that $\epsilon_1 + U_1/2$ is the energy zero point.

As shown in Fig. 2, when the spin bias $V_1 = 0$, the electron number will be 0, 1, and 2 if μ_1 is well below ϵ_1 , between $[\epsilon_1, \epsilon_1 + U_1]$, and above $\epsilon_1 + U_1$. The empty, singly-occupied, and doubly-occupied unpolarized regimes are denoted by **E0**, **S0**, and **D0**, respectively. Each regime develops into two spin-polarized regimes when a positive ($V_1 > 0$) or negative ($V_1 < 0$) spin bias is applied. **E0** \rightarrow **S \uparrow 1**, **S \downarrow 1**; **S0** \rightarrow **S \uparrow 2**, **S \downarrow 2**; **D0** \rightarrow **S \uparrow 3**, **S \downarrow 3**. We denote the 9 regimes by the electron number and polarization. 0, \uparrow , and \downarrow stand for unpolarized, spin-up and spin-down, respectively. For example, **S \uparrow 2** represents the second regime when the dot 1 is singly-occupied and \uparrow polarized. We describe the 9 regimes one by one as follows.

E0 Both $\mu_{1\uparrow}$ and $\mu_{1\downarrow}$ are well below ϵ_1 , then the dot is empty and unpolarized.

S \uparrow 1 Applying a positive spin bias to **E0** till $\mu_{1\uparrow}$ is above ϵ_1 while $\mu_{1\downarrow}$ still below ϵ_1 , so only an electron of spin-up is energetically allowed to occupy the dot. The spin in the dot 1 is \uparrow polarized.

S \downarrow 1 Opposite to **S \uparrow 1** by applying a negative spin bias.

S0 Both $\mu_{1\uparrow}$ and $\mu_{1\downarrow}$ are between ϵ_1 and $\epsilon_1 + U_1$. At least one electron can be filled into the dot. But either $\mu_{1\uparrow}$ or $\mu_{1\downarrow}$ can not compensate the charge energy U_1 for filling the second electron. The opportunity of occupation for spin up or down electron is the same. Therefore the electron spin is unpolarized.

S \uparrow 2 Applying a positive spin bias to **S0** until $\mu_{1\downarrow}$ is well below ϵ_1 or $\mu_{1\uparrow}$ is well above $\epsilon_1 + U_1$. The former situation is similar to **S \uparrow 1**. In the latter situation, if the dot is initially occupied by a \downarrow spin, an \uparrow spin can still enter the dot because $\mu_{1\uparrow} > \epsilon_1 + U_1$. Once the \uparrow enter the dot, the \downarrow will be repulsed out of the dot and unable to enter again because $\mu_{1\downarrow} < \epsilon_1 + U_1$, cannot supply enough charge energy. Both situations lead to a spin \uparrow electron filled in the dot.

S \downarrow 2 Opposite to **S \uparrow 2** by applying a negative spin bias.

D0 Both $\mu_{1\uparrow}$ and $\mu_{1\downarrow}$ are well above $\epsilon_1 + U_1$, the dot is occupied by two electrons, one up and the other down due to the Pauli exclusive principle. So there is no polarization.

S \uparrow 3: $\mu_{1\uparrow}$ is well above $\epsilon_1 + U_1$ while $\mu_{1\downarrow}$ is below $\epsilon_1 + U_1$.

S \downarrow 3 Opposite to **S \uparrow 3**.

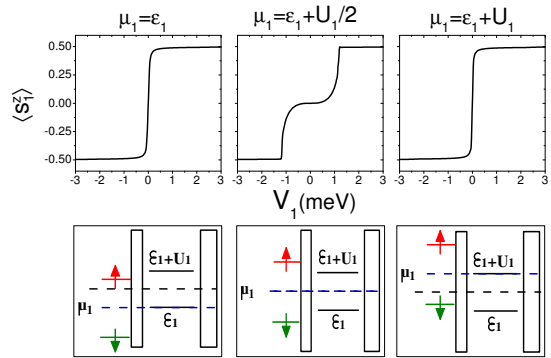


FIG. 3: (Color online) $\langle s_1^z \rangle$ vs V_1 when μ_1 is aligned with ϵ_1 , $\epsilon_1 + U_1/2$, and $\epsilon_1 + U_1$. Notice that for the first and the last cases, $\langle s_1^z \rangle$ is immediately reversed between $\sim 1/2$ and $\sim -1/2$ when spin bias V_1 is changed from positive to negative over a width $\sim \Gamma_1$.

Moreover, as shown in Fig. 3, at two conditions when μ_1 is aligned with ϵ_1 , or $\epsilon_1 + U_1$, the maximal polarization can be achieved immediately as long as the spin bias V_1 overwhelms Γ_1 , the broadening of the dot level due to the dot-lead coupling. In both situations there is only one electron in the dot. So if the dot is weakly coupled to the leads, one can manipulate the single spin by using a small spin bias. $\mu_1 = \epsilon_1 + U_1/2$ in Fig.3 represents the hardest condition to polarize the spin, in which the spin bias has to overcome intra-dot Coulomb repulsion energy.

D. Discussion

We have shown that the quantum spin in the dot 1 can be well controlled and maintained by using a large spin bias V_1 . We argue that this control is robust once the magnitude of V_1 energetically overwhelms those of decoherence mechanisms, such as hyperfine interaction with nuclear spins of host materials, or spin-orbital coupling. As shown in Fig. 2, the edges between different regimes are very sharp because Γ_1 is much smaller than U_1 . Increasing the dot-lead coupling will blur the edges, and lower the efficiency of manipulation.

According to our calculation based on the semiconductor QD,³⁵ the order of the spin biases required for the manipulation is about 0.1 – 1meV, which should be within touch of the experiments. For example, Zaffalon and van Wees³⁶ reported that the spin-polarized current injected from Co electrodes to an Al island had induced a splitting $\mu_{\uparrow} - \mu_{\downarrow} = eIR_s/P$, where $I \sim 10 - 100\mu A$ is the injection current, $P = 7\%$ is the spin injection efficiency of the Co/Al tunnel barrier, and R_s is a defined quantity of dimension of resistance, which was measured up to 250m Ω at 4.2K. Therefore the spin bias in this experiment can be as large as $e \times 0.1mA \times 250m\Omega / 0.07 \sim$

0.35meV. Although it is not explicitly addressed in the publications^{13,14,15,18,19,37} to our knowledge, the values of the spin-dependent chemical potential splitting in semiconductors may be larger than those in metals, based on the following two arguments. First, the density of states (DOS) near the Fermi level is much smaller in semiconductors. The same imbalance of one spin component than the other should occupy wider range in energy. Second, the measured spin diffusion lengths in semiconductors are usually $\sim 1 - 10\mu\text{m}$,³⁷ much longer than those in metals (\sim hundreds of nm),³⁸ so the spin accumulation in semiconductors are more robust to maintain the spin bias.

III. MEASUREMENT OF QUANTUM SPIN BY MEANS OF SPIN BIAS

After generating the quantum spin in the dot 1, one needs to read it out to examine the outcome. Experimentally, the read-out of single spin has been achieved by various of spin-to-charge conversion techniques, such as single-shot readout using energy⁷ or tunneling rate⁸ difference, and Pauli spin blockade.⁵ All these techniques require the trapped spin to leave its host dot, which, however, should be avoided if the polarized spin is used for quantum computation or memory (for example initialization of a qubit). Here we propose an alternative solution, in which an additional quantum dot (dot 2) is located at the vicinity of the dot 1. Due to the spin correlation between the two dots, the spin polarization of the dot 1 can be measured by probing the spin-dependent transport through the dot 2. This approach looks like a spin version of charge sensing technique,^{2,3} or spin sensing technique. Moreover, we demonstrate that the net electric current generated by applying a small spin bias to the dot 2 is proportional to $T_{2\uparrow} - T_{2\downarrow}$, where $T_{2\sigma}$ is the transmission probability for spin σ electrons. Therefore the spin-dependent transport through the dot 2 can be explored by applying a very small spin bias V_2 to it, instead of by using ferromagnetic electrodes.

A. The model for the coupled quantum dots

Now our model consists of two quantum dots (Fig.1), each dot is coupled independently to its leads. Like the dot 1, the dot 2 is also described by the Anderson model coupled to two metallic leads

$$\begin{aligned}
 H_2 = & \sum_{\sigma} \epsilon_2 n_{2\sigma} + U_2 n_{2\uparrow} n_{2\downarrow} \\
 & + \sum_{k,\alpha,\sigma} \epsilon_{k\alpha\sigma} c_{k\alpha\sigma}^{\dagger} c_{k\alpha\sigma} + \sum_{k,\alpha,\sigma} (V_{k\alpha\sigma} c_{k\alpha\sigma}^{\dagger} d_{2\sigma} + h.c.).
 \end{aligned}
 \tag{2}$$

The two dots are assumed to be coupled weakly to each other. Basically, there are three kinds of interactions between two quantum dots:

1) The tunneling coupling ($t_c d_{1\sigma}^{\dagger} d_{2\sigma} + h.c.$).³⁹ When the two dots are very closely located electrons are allowed to tunnel between the two dots directly. It should be avoided if one intends to perform a noninvasive measurement;

2) The capacitive coupling $U' n_1 n_2$.⁴⁰ The Coulomb repulsive interaction always exists when the two dots are closely located, but well separated. The occupancy of electrons in one dot will affect the charge transport in another dot. This is the microscopic mechanism for the charge sensing technique. However it is not spin-resolved, and we shall ignore it in our calculation.

3) The Heisenberg exchange coupling

$$V_{12} = J \mathbf{s}_1 \cdot \mathbf{s}_2 \tag{3}$$

where $\mathbf{s}_i = \frac{1}{2} \sum_{\sigma,\sigma'} d_{i\sigma}^{\dagger} \hat{\sigma}_{\sigma\sigma'} d_{i\sigma'}$ and $\hat{\sigma} = (\sigma_x, \sigma_y, \sigma_z)$ are the Pauli matrices.³⁵ It does not change the occupation number of each dot, but affects the states of electron spin, in particular when electrons are spin-resolved.

To simplify our calculation, we only consider the exchange coupling. The total Hamiltonian for the whole system becomes

$$H = H_1 + H_2 + V_{12}. \tag{4}$$

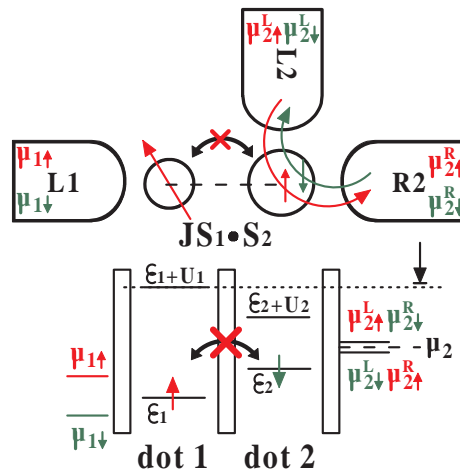


FIG. 4: (Color online) Schematic illustration and energy configuration of the low-energy effective double-dot model. The inter-dot first order direct tunneling is suppressed due to careful design of all characteristic energies. The second order virtual hopping induces a low-energy Heisenberg exchange interaction with a considerable positive exchange strength J . $\mu_{2\sigma}^{\alpha}$ is the Fermi level for spin $\sigma (\in \{\uparrow, \downarrow\})$ electrons in the $\alpha (\in \{L2, R2\})$ lead of the dot 2. $\mu_2 = \frac{1}{2}(\mu_{2\uparrow}^{L/R} + \mu_{2\downarrow}^{L/R})$ is the shared middle point of Fermi levels for both leads L2 and R2.

We have to point out that the model in Eq. (4) with considerable J is valid in experiments only as a low-energy effective Hamiltonian when direct electron hoppings are quenched between two tunneling-coupled quantum dots (coupling constant t_c can be as large as hundreds of μeV).^{35,41} To suppress the direct tunneling and

only to employ the low-energy spin dynamics between the two dots, the energy configuration of the double-dot should be carefully designed as shown in Fig. 4. The level energies of the two dots can be adjusted respect to each other by tuning gate voltages, while the charging energies of two dots can be customized by engineering dot sizes.³⁵ We choose such an energy configuration that $\epsilon_2 - \epsilon_1 > |t_c|$ and $(\epsilon_1 + U_1) - (\epsilon_2 + U_2) > |t_c|$. For the dot 1, μ_1 and V_1 are restricted to the singly-occupied regimes shown in Fig. 2. Moreover, since $\epsilon_1 < \epsilon_2$, the electron in the dot 1, which resides on ϵ_1 , cannot hop to the dot 2 no matter whether the dot 2 is occupied or not. For the dot 2, the scanning range of its middle point of the Fermi level μ_2 is well restricted $< \epsilon_1 + U_1$ (as shown by the dotted line in Fig. 4). As a result, although double occupation in the dot 2 is allowed when $\mu_2 > \epsilon_2 + U_2$, the electrons in the dot 2 cannot acquire enough charging energy from its leads to hop to the dot 1. The above conditions assure that there is no direct hopping between the two dots. However, the second order virtual hopping between the two dots is still possible to happen. As a result, the low-energy correlation between the two dots is well described by the Heisenberg Hamiltonian with a positive exchange coupling strength J . Using the simplest Hubbard model estimate $J = \frac{4t_c^2}{U}$, J can be as large as 0.09 meV when $t_c = 0.15\text{meV}$ and $U \sim 1\text{meV}$.³⁵

B. Effective Field Approximation

In the presence of the exchange interaction, once the electron in the dot 1 is polarized by a large spin bias, it will act approximately as an effective magnetic field, and weakly polarize the electron in the nearby dot 2. The polarized spin in the dot 2 will in turn act as an effective magnetic field to the dot 1, and will influence the polarization of the dot 1. If there is no extra mechanism to break the spin symmetry, this self-consistent process repeats until $\langle s_1^z \rangle$ and $\langle s_2^z \rangle$ approach to zero, where $\langle s_i^z \rangle \equiv \frac{1}{2}(\langle n_{i\uparrow} \rangle - \langle n_{i\downarrow} \rangle)$ is the spin polarization in the dot i . However, because of the large spin bias V_1 applied to the dot 1, $\langle s_1^z \rangle$ and $\langle s_2^z \rangle$ will finally saturate at certain values other than 0. Besides, the magnitude of the effective magnetic field generated by the dot 2 is of the order $\sim J\langle s_2^z \rangle$ which, if small enough ($\ll V_1$), will hardly affect the spin polarization in the dot 1. In this limit, our calculation in the Sec. II, which does not include the spin correlation between the dots 1 and 2, is still valid. Besides, in the following calculations of the physical quantities of the dot 2 we treat the spin of the dot 1 as an effective magnetic field using the Hamiltonian

$$V_{12} = \frac{J}{2}s_1^- d_{2\uparrow}^\dagger d_{2\downarrow} + \frac{J}{2}s_1^+ d_{2\downarrow}^\dagger d_{2\uparrow} + \frac{J}{2}s_1^z (n_{2\uparrow} - n_{2\downarrow}), \quad (5)$$

where $s_1^{z,+,-}$ are quantum field operators. It is worth stressing that the self-consistent calculation is very complicated, but still available in the present problem. To

avoid the mathematics, the present approximation is believed to give an intuitive picture how the spin bias is converted into a charge signal.

We have to point out that our approximation in Eqs. (1), (2), and (6) are valid only when the spin biases applied to the dots 1 and 2 satisfy

$$V_1 \gg J\langle s_2^z \rangle, \quad J\langle s_1^z \rangle \gg V_2, \quad (6)$$

which means that 1) the spin polarization in the dot 1 is dominantly determined by the spin bias V_1 applied to the leads attached to it; 2) the polarization of the dot 2 is dominantly determined by its spin correlation with the dot 1. The first requirement is easily satisfied. The bias voltage applied to a quantum dot can be as large as several meV.⁴ In our calculation, V_1 is taken to be of order of meV. Generally, $\langle s_2^z \rangle$ must $\in [-0.5, 0.5]$ (as shown in Fig. 6, $|\langle s_2^z \rangle|$ is actually less than 0.2 in our results). We choose $J < 0.1\text{meV}$, so $J\langle s_2^z \rangle$ is almost two orders smaller than V_1 . The second requirement is limited by the smallest current measurable in experiment. The conductance through a quantum dot is of the order of $\frac{2e^2}{h} \approx 7.75 \times 10^{-5}\Omega^{-1}$, while the current measured in QD experiment can be as accurate as down to $\Delta I \sim \text{pA}$ even ten years ago.⁴² So the minimum bias voltage required to generate such a small current is of the order of $\Delta I / \frac{2e^2}{h} = \text{pA} / (7.75 \times 10^{-5}\Omega^{-1}) \sim \mu\text{V}$, which is orders smaller than the reported value of J estimated using the Hubbard model in the parallel-coupled double-quantum-dot experiment ($\sim 90\mu\text{eV}$).³⁵

C. Spin-dependent transport and Green's function technique

To explore the spin-resolved transport of the dot 2 we calculate its spin conductance, which is defined as the ratio of the charge current to the spin bias.^{29,30,31} To define the spin conductance, we assume that a very small spin bias V_2 is applied to the two leads of the dot 2. When there is no spin and charge biases, the Fermi level of electrodes attached to the dot 2 is denoted as μ_2 . The spin bias V_2 is defined as the spin splitting of Fermi levels for electrons in the left lead

$$\mu_{2\uparrow/\downarrow}^L = \mu_2 \pm V_2/2,$$

and in the right lead

$$\mu_{2\uparrow/\downarrow}^R = \mu_2 \mp V_2/2.$$

In the presence of the pure spin bias V_2 , electrons of spin \uparrow and \downarrow will flow along opposite directions through the dot 2. If the up-down symmetry of electron spin in the dot is not broken, electric currents of spin \uparrow and \downarrow will cancel with each other. Consequently a pure spin current is formed.⁴³ However, if the spin symmetry of the dot 2 is broken, the pure spin bias V_2 applied to the dot 2 will generate a net electric current. We thus define the spin

conductance as the ratio between the net current and the pure spin bias in the limit of the zero spin bias. In Appendix A, we derive the formula of spin conductance at zero temperature,

$$G^s(\mu) = \lim_{V^s \rightarrow 0} \frac{\partial(I_\uparrow + I_\downarrow)}{\partial V^s} = \frac{e^2}{h} [T_\uparrow(\mu) - T_\downarrow(\mu)], \quad (7)$$

where $T_{2\sigma}$ is the transmission probability for σ electrons through the dot 2 in the framework of linear response theory. Therefore numerical results presented in Secs. III D and III E are given only in terms of $T_{2\uparrow} - T_{2\downarrow}$ in the unit of $\frac{e^2}{h}$.

In the linear response theory, the σ component of transmission probability is given by⁴⁴

$$T_{2\sigma}(\mu_2) = [G_{2\sigma}^r(\omega)\Gamma_2^L(G_{2\sigma}^r(\omega))^\dagger\Gamma_2^R]_{\omega=\mu_2},$$

where the retarded Green's function $G_2^r(\omega)$ is defined as the Fourier transform of

$$G_{2\sigma}^r(t) = -i\theta(t)\langle\{d_{2\sigma}(t), d_{2\sigma}^\dagger\}\rangle$$

with $d_{2\sigma}(t) = e^{i(H_2+V_{12})t}d_{2\sigma}e^{-i(H_2+V_{12})t}$. $\Gamma_2^\alpha = \sum_k 2\pi|V_{k\alpha\sigma}|^2 2\pi\delta(\omega - \epsilon_{k\alpha\sigma})$ is the broadening of the dot 2 level ϵ_2 due to the couplings to the α lead. Using the equation-of-motion of $G_{2\sigma}^r$ with respect to $H_2 + V_{12}$ in Eq. (2), we arrive at (detailed deductions and approximations are given in Appendix B)

$$\begin{pmatrix} \Omega & -\frac{J}{2} & -\frac{J}{2} \\ -\frac{J}{8} & \Omega & \frac{J}{4} \\ -\frac{J}{4} & \frac{J}{2} & \Omega + \frac{J}{4} \end{pmatrix} \begin{pmatrix} G_{2\uparrow}^r \\ G_2 \\ G_3 \end{pmatrix} = \begin{pmatrix} 1 + UG_4 \\ \langle s_1^z \rangle + UG_5 + \frac{J}{2}G_6 \\ JG_5 + \frac{J+2U}{2}G_6 \end{pmatrix},$$

$$\begin{pmatrix} \Omega - U & -\frac{J}{2} & -\frac{J}{2} \\ -\frac{J}{8} & \Omega - U & -\frac{J}{4} \\ -\frac{J}{4} & -\frac{J}{2} & \Omega - \frac{J+4U}{4} \end{pmatrix} \begin{pmatrix} G_4 \\ G_5 \\ G_6 \end{pmatrix} = \begin{pmatrix} N_1 \\ N_2 \\ N_3 \end{pmatrix},$$

$$\begin{pmatrix} \Omega & \frac{J}{2} & -\frac{J}{2} \\ \frac{J}{8} & \Omega & -\frac{J}{4} \\ -\frac{J}{4} & -\frac{J}{2} & \Omega + \frac{J}{4} \end{pmatrix} \begin{pmatrix} G_{2\downarrow}^r \\ G_8 \\ G_9 \end{pmatrix} = \begin{pmatrix} 1 + UG_{10} \\ \langle s_1^z \rangle + UG_{11} - \frac{J}{2}G_{12} \\ -JG_{11} + \frac{J+2U}{2}G_{12} \end{pmatrix},$$

$$\begin{pmatrix} \Omega - U & \frac{J}{2} & -\frac{J}{2} \\ \frac{J}{8} & \Omega - U & \frac{J}{4} \\ -\frac{J}{4} & \frac{J}{2} & \Omega - \frac{J+4U}{4} \end{pmatrix} \begin{pmatrix} G_{10} \\ G_{11} \\ G_{12} \end{pmatrix} = \begin{pmatrix} N_4 \\ N_5 \\ N_6 \end{pmatrix}, \quad (8)$$

where we denote $\Omega = \omega - \epsilon_2 + \frac{i}{2}\Gamma_2$, $\Gamma_2 = \Gamma_2^L + \Gamma_2^R$. $G_2 = \langle\langle d_{2\uparrow}s_1^z | d_{2\uparrow}^\dagger \rangle\rangle$, $G_3 = \langle\langle d_{2\downarrow}s_1^- | d_{2\uparrow}^\dagger \rangle\rangle$, $G_4 = \langle\langle d_{2\uparrow}n_{2\downarrow} | d_{2\uparrow}^\dagger \rangle\rangle$, $G_5 = \langle\langle d_{2\uparrow}n_{2\downarrow}s_1^z | d_{2\uparrow}^\dagger \rangle\rangle$, $G_6 = \langle\langle d_{2\downarrow}n_{2\uparrow}s_1^- | d_{2\uparrow}^\dagger \rangle\rangle$, $G_8 = \langle\langle d_{2\downarrow}s_1^z | d_{2\downarrow}^\dagger \rangle\rangle$, $G_9 = \langle\langle d_{2\uparrow}s_1^+ | d_{2\downarrow}^\dagger \rangle\rangle$, $G_{10} = \langle\langle d_{2\downarrow}n_{2\uparrow} | d_{2\downarrow}^\dagger \rangle\rangle$, $G_{11} = \langle\langle d_{2\downarrow}n_{2\uparrow}s_1^z | d_{2\downarrow}^\dagger \rangle\rangle$, $G_{12} = \langle\langle d_{2\uparrow}n_{2\downarrow}s_1^+ | d_{2\downarrow}^\dagger \rangle\rangle$, where the notation $\langle\langle A|B \rangle\rangle$ stands for the Fourier transform of the retarded Green's function $-i\theta(t)\langle\{A(t), B\}\rangle$. $N_1 = \langle n_{2\downarrow} \rangle$, $N_2 = \langle n_{2\downarrow}s_1^z \rangle$, $N_3 = -\langle d_{2\uparrow}^\dagger d_{2\downarrow}s_1^- \rangle$, $N_4 = \langle n_{2\uparrow} \rangle$, $N_5 = \langle n_{2\uparrow}s_1^z \rangle$, $N_6 = -\langle d_{2\downarrow}^\dagger d_{2\uparrow}s_1^+ \rangle$. It is worth pointing

out that our deduction is similar to the previous work,⁴⁵ however our calculation retains $\langle s_1^z \rangle$ as an input parameter ranging from -0.5 to 0.5, reflecting the spin polarization in the dot 1 to be detected.

Using the identity of Green's functions at equilibrium^{33,34}

$$\mathbf{G}^< = i\mathbf{A}f, \quad \mathbf{A} = -2\text{Im}\mathbf{G}^r,$$

where \mathbf{A} is the spectral function, we self-consistently calculate expectation values in Eqs. (8), for example

$$\begin{aligned} \langle d_{2\uparrow}^\dagger d_{2\downarrow} s_1^- \rangle &= -i\langle\langle d_{2\downarrow}(t)s_1^-(t) | d_{2\uparrow}^\dagger(t') \rangle\rangle_{t=t'}^< \\ &= -i \int \frac{d\omega}{2\pi} \langle\langle d_{2\downarrow}s_1^- | d_{2\uparrow}^\dagger \rangle\rangle_\omega^< \\ &= -\frac{1}{\pi} \int d\omega f_2(\omega) \text{Im}\langle\langle d_{2\downarrow}s_1^- | d_{2\uparrow}^\dagger \rangle\rangle, \end{aligned} \quad (9)$$

where

$$f_2 = \frac{1}{e^{(\omega-\mu_2)/k_B T} + 1}.$$

D. Numerical results

For numerical calculations, we choose a set of parameters in consistence with the parallel-coupled double-quantum-dot experiment by Chen *et al.*,³⁵ $k_B T = 0.004$ meV, $J = 0.09$ meV, $U_2 = 0.8$ meV, and $\Gamma_2^\sigma = 0.0375$ meV. We set $\epsilon_2 = -0.4$ meV to assure that $\epsilon_1 + U_1/2 = \epsilon_2 + U_2/2$ is the zero point of energy. Despite the above experiment parameters lead to the Kondo effect at low temperatures,³⁵ we have enough reasons to rule it out from the present considerations. For the dot 1, the spin is polarized by the large spin bias V_1 , thus Kondo effect is usually quenched. For the dot 2, later we will see the results are meaningful only when μ_2 is around the ϵ_2 and $\epsilon_2 + U_2$, where the first-order tunneling between the leads L2 and R2 through the dot 2 is dominant and suppresses the Kondo effect.

We assume that there is an unknown spin in the dot 1 to be detected, i.e. all the \mathbf{S} regimes in Fig. 2. The states of the dot 2 and the double-dot are classified by the electron occupation as shown in Tab. I for $J > 0$. The one-electron state of the double-dot is also the empty state (0) of the dot 2. The doubly-occupied states (D) of the dot 2 are two-fold degenerate triply-occupied states of the double-dot. The singly-occupied state of the dot 2, due to the exchange interaction, could favor parallel (P) or anti-parallel (AP) alignment with the spin in the dot 1. Our numerical results show that the state energies of these two possible alignments happen to be equal to those for the singlet and triplets states of the double-dot,

$$E_1^{\text{AP}} = \langle S | H_2^{\text{iso}} + V_{12} | S \rangle = \epsilon_2 - \frac{3}{4}J,$$

and

$$E_1^{\text{P}} = \langle T_{0,\pm} | H_2^{\text{iso}} + V_{12} | T_{0,\pm} \rangle = \epsilon_2 + \frac{1}{4}J,$$

where $H_2^{\text{iso}} = \epsilon_2 n_2 + U_2 n_{2\uparrow} n_{2\downarrow}$, and

$$\begin{aligned} S &= \frac{1}{\sqrt{2}}(|\uparrow\rangle_2 |\downarrow\rangle_1 - |\downarrow\rangle_2 |\uparrow\rangle_1) \\ T_0 &= \frac{1}{\sqrt{2}}(|\uparrow\rangle_2 |\downarrow\rangle_1 + |\downarrow\rangle_2 |\uparrow\rangle_1) \\ T_+ &= |\uparrow\rangle_2 |\uparrow\rangle_1, \quad T_- = |\downarrow\rangle_2 |\downarrow\rangle_1. \end{aligned} \quad (10)$$

Because the singlet is the anti-parallel alignment of the two spins while three triplets are in parallel alignments, it is no wonder that the AP state at the energy of the singlet favors anti-parallel alignment while the P states at the energy of triplets prefer parallel. We emphasize here that despite energetically equal, the P and AP states are not equivalent to the triplets and singlet states, because the singlet and triplets are nonsense in spin-polarized situations.

TABLE I: When assuming there is an electron in the dot 1, the energy spectrum of the dot 2 for $J > 0$. Where P or AP corresponds to the alignment of two spins favoring parallel or anti-parallel. One just exchanges the anti-parallel and parallel to have the $J < 0$ case.

electron number			
in double-dot	1	2	3
electron number			
in dot 2	0	1	2
Ground state	Empty(0) $E_0 = 0$	Anti-parallel(AP) $E_1^{\text{AP}} = \epsilon_2 - \frac{3}{4}J$	Double(D) $E_2 = 2\epsilon_2 + U_2$
Excited states		Parallel(P) $E_1^{\text{P}} = \epsilon_2 + \frac{1}{4}J$	

The poles of Green's functions of the dot 2 reflect the energies required for transitions between these states with different occupancies of electrons. When the Fermi surface of leads are aligned with these poles and supply the required energy, the transitions will take place, giving rise to a conductance peak. We list the four possible transitions to fill the dot 2 with $0 \rightarrow 1 \rightarrow 2$ electrons when $J > 0$ in Table. II, together with the energies required by the transitions and the corresponding charge conductance peaks in Fig. 5.

TABLE II: Transitions between states with different particle numbers in the dot 2 when $J > 0$, energies required from the Fermi surface to supply the transitions, and the corresponding conductance peaks in Fig. 5.

Transitions	Required energies	Peaks in Fig. 5
$0 \rightarrow \text{AP}$	$E_1^{\text{AP}} - E_0 = \epsilon_2 - \frac{3}{4}J$	1 (left)
$0 \rightarrow \text{P}$	$E_1^{\text{P}} - E_0 = \epsilon_2 + \frac{1}{4}J$	2
$\text{P} \rightarrow \text{D}$	$E_2 - E_1^{\text{P}} = \epsilon_2 + U_2 - \frac{1}{4}J$	3
$\text{AP} \rightarrow \text{D}$	$E_2 - E_1^{\text{AP}} = \epsilon_2 + U_2 + \frac{3}{4}J$	4 (right)

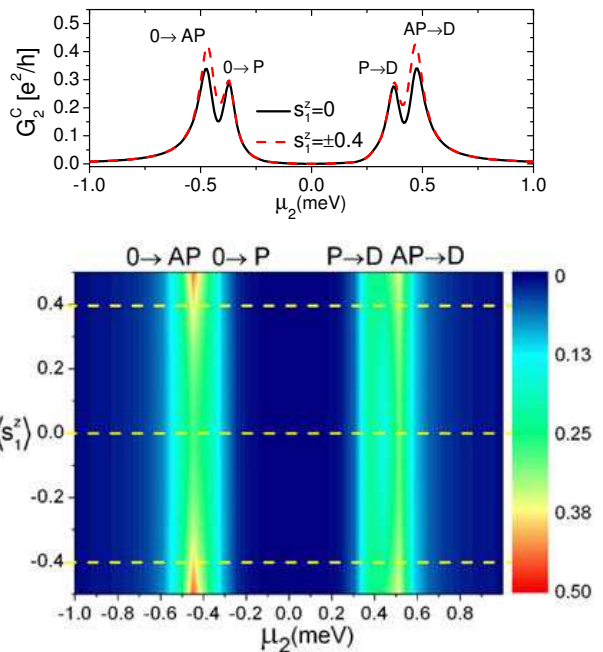


FIG. 5: (Color online) The charge conductance ($\frac{e^2}{h}(T_{2\uparrow} + T_{2\downarrow})$) vs μ_2 and $\langle s_1^z \rangle$. μ_2 is the Equilibrium Fermi level. The exchange coupling strength $J = 0.09$ meV, $U_2 = 0.8$ meV. $\epsilon_2 = -0.4$ meV, $\Gamma_2^0 = 0.0375$ meV. The upper panel shows the values along the horizontal dashed lines in the lower panel.

There are four charge conductance peaks in Fig. 5, forming two groups spaced by U_2 . The peaks in each group are separated by J . When $\langle s_1^z \rangle = 0$, the numerical results are in good agreement with those by Tolea and Bulka.⁴⁵ From the above results, one understands why we ignore the inter-dot capacitive repulsion $U'n_1n_2$. In the singly-occupied regime of the dot 1, this term adds a U' to the singly-occupied energy, and $2U'$ to the doubly-occupied energy of the dot 2, so it only widens the spacing between the peaks 1 and 2 respect to 3 and 4 by U' in the conductance spectrum of the dot 2, and does not contribute to any spin-dependent effect.

Interesting results emerge when $\langle s_1^z \rangle \neq 0$. As an example, we consider the case $\langle s_1^z \rangle > 0$, i.e. an \uparrow electron is in the dot 1. We start with the empty state of the dot 2, i.e. μ_2 is well below the energy of $0 \rightarrow \text{AP}$ transition at $\epsilon_2 - 3J/4$. When μ_2 is raised to be aligned with the transition pole $0 \rightarrow \text{AP}$, the dot 2 will favor \downarrow electron occupation because of the \uparrow electron in the dot 1. As shown in Fig. 6, the difference $(n_{2\downarrow} - n_{2\uparrow})$ and $\langle s_2^z \rangle$ reach maximum after μ_2 is above the transition $0 \rightarrow \text{AP}$ at $\epsilon_2 - 3J/4$. The transport of \downarrow (\uparrow) electrons through the dot 2 via $0 \rightarrow \text{AP}$ thus will be enhanced (suppressed), i.e. $T_{2\uparrow} - T_{2\downarrow} < 0$, which accounts for the negative value region around $\epsilon_2 - 3J/4$ (transition $0 \rightarrow \text{AP}$) in Fig. 6 when $\langle s_1^z \rangle > 0$. Continue raising μ_2 until aligned with the transition $0 \rightarrow \text{P}$ at $\epsilon_2 + J/4$, the electron in the dot 2 could be either \uparrow or \downarrow because both situations are ener-

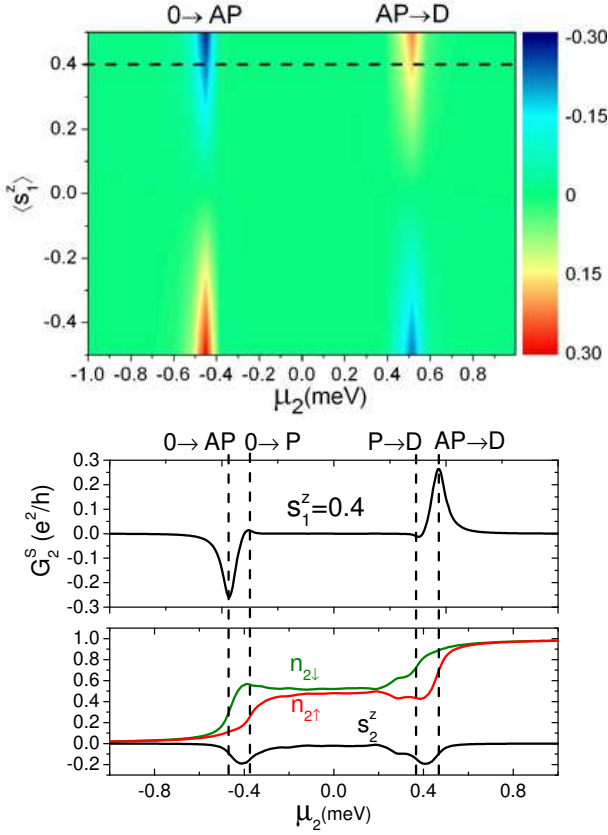


FIG. 6: (Color online) The spin conductance ($\frac{e^2}{h}(T_{2\uparrow} - T_{2\downarrow})$) vs μ_2 and $\langle s_1^z \rangle$. μ_2 is the Equilibrium Fermi level. The parameters are the same as those in Fig. 5. The lower panel shows the values along the horizontal dashed line in the higher panel.

getically allowed. A direct result of this nearly arbitrary spin polarization is that the second electron added to the dot 2 via the transition $P \rightarrow D$ can also be either \uparrow or \downarrow . So no spin orientation is particularly favored when electrons tunnel via the transitions $0 \rightarrow P$ at $\epsilon_2 + \frac{1}{4}J$ and $P \rightarrow D$ at $\epsilon_2 + U_2 - \frac{1}{4}J$. As a result, $n_{2\downarrow} - n_{2\uparrow}$ approaches to zero between $\epsilon_2 + \frac{1}{4}J$ and $\epsilon_2 + U_2 - \frac{1}{4}J$, and there is only invisible difference between $T_{2\uparrow}$ and $T_{2\downarrow}$ at both energies. If the second electron is added via the transition $AP \rightarrow D$ at $\epsilon_2 + U_2 + \frac{3}{4}J$, it will automatically favor \uparrow because there is already a \downarrow electron in the dot 2. This process is clearly shown as $n_{2\downarrow} - n_{2\uparrow}$ reaches maximum between $\epsilon_2 + U_2 - \frac{1}{4}J < \mu_2 < \epsilon_2 + U_2 + \frac{3}{4}J$ and finally goes to zero after $\mu_2 > \epsilon_2 + U_2 + \frac{3}{4}J$. So $T_{2\uparrow} - T_{2\downarrow} > 0$ when μ_2 is aligned with the transition $AP \rightarrow D$ at $\epsilon_2 + U_2 + \frac{3}{4}J$.

By the same token, the case $\langle s_1^z \rangle < 0$ can be calculated. In Fig. 7, we compare the charge and spin conductances as functions of $\langle s_1^z \rangle$ at $\mu_2 = \epsilon_2 - 3J/4$ ($0 \rightarrow AP$) and $\epsilon_2 + J/4$ ($0 \rightarrow P$). The major difference is that at $0 \rightarrow AP$, $T_{2\uparrow} - T_{2\downarrow}$ changes sign as $\langle s_1^z \rangle$ turns from positive to negative polarization, while $T_{2\uparrow} + T_{2\downarrow}$ remains positive.

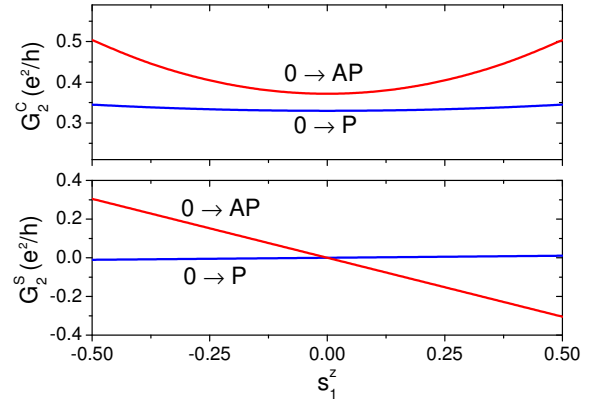


FIG. 7: (Color online) The charge conductance ($T_{2\uparrow} + T_{2\downarrow}$) and spin conductance ($T_{2\uparrow} - T_{2\downarrow}$) vs $\langle s_1^z \rangle$ when $\mu_2 = \epsilon_2 - 3J/4$ ($0 \rightarrow AP$) and $\epsilon_2 + J/4$ ($0 \rightarrow P$). The other parameters are the same as in Figs. 5 and 6.

Therefore, the spin conductance of the dot 2 provides a practical tool to probe the spin polarization in the dot 1.

E. Model study when $J < 0$

The case of $J < 0$ is different from that of $J > 0$, because in this situation the ground states favors the parallel alignment of two spins in the two dots. Since there is no corresponding experiment data for $J < 0$, we just assume a set of model parameters in analogy to those when $J > 0$. In the charge conductance \mathcal{G}_2^C of Fig. 8, only two peaks are clearly visible, they come from the transitions $0 \rightarrow P$ and $P \rightarrow D$. The conductance peaks for $0 \rightarrow AP$ and $AP \rightarrow D$ are suppressed. Unlike the P states, which actually originate from the 3-fold triplets when $s_1^z = 0$, there is only one AP state. The contribution of AP to conductance as an excited state is too weak compared to those of P states, in particular as the dot 2 is weakly coupled to the leads.⁴⁵ As we see in Fig. 5, the peak maximum of the AP state as the ground state and the total three P states as the excited states are roughly of the same order, so the peak maximum of $0 \rightarrow AP$ in \mathcal{G}_2^C of Fig. 8 as the excited state should be about one order (3×3) smaller than that of the P states as the ground state.

For the spin conductance \mathcal{G}_2^S in Fig. 8, two changes occur when compared with Fig. 6. The first is that the peak and dip positions move to $E_1^P - E_0 = \epsilon_2 + \frac{1}{4}J$ and $E_2 - E_1^P = \epsilon_2 + U_2 - \frac{1}{4}J$, because the P states are one-electron ground states for the dot 2 when $J < 0$. The second is that the spin conductance changes sign respect to Fig. 6 because the first electron that enters the dot 2 tends to be parallel-aligned with the spin in the dot 1 when $J < 0$, in contrast to the anti-parallel when $J > 0$.

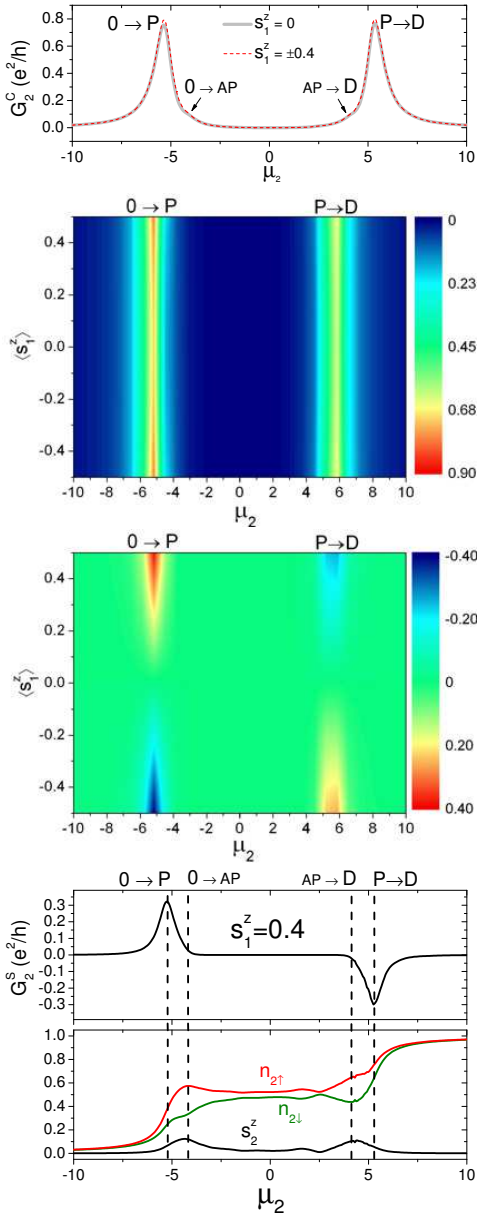


FIG. 8: (Color online) The charge conductance ($\frac{e^2}{h}(T_{2\uparrow} + T_{2\downarrow})$, top two panels) and the spin conductance ($\frac{e^2}{h}(T_{2\uparrow} - T_{2\downarrow})$, bottom two panels) vs μ_2 and $\langle s_1^z \rangle$ for negative exchange coupling J . The parameters $J = -1$, $\epsilon_2 = -5$, $U_2 = 10$, $\Gamma_2 = 1$.

IV. SUMMARY

We investigated a double-quantum-dot system, coupled to electrodes with spin-dependent splitting of chemical potentials (spin bias). Using a large spin bias, the quantum spin in the dot 1 can be manipulated and maintained in a pure electric manner. The parameters and regimes of the manipulation were discussed in details. When an inter-dot exchange coupling is taken into account, the ground state of the two spins singly occupied

in each dot tends to form an anti-parallel or parallel alignment, depending on the coupling constant J positive or negative. The spin-dependent transport through the dot 2 thus can be used to detect the polarization of spin in the dot 1 nondestructively. We found that the measurement of the spin-dependent transport can be realized by measuring the net electric current under a spin bias, which defines a spin conductance. We observed that the spin conductance of the dot 2 changes its sign as the orientation of spin in the dot 1 reverses, much more sensitive than the usual charge conductance. The two cases demonstrate that the spin bias may be a promising approach to manipulate a single spin while allowing this manipulation to be monitored in quantum dot systems. Finally, as a summary, we compare our model with the charge sensing technique^{2,3} in Table III.

V. ACKNOWLEDGEMENTS

We thank Q. F. Sun, R. Lü, Y. J. Bao, B. Zhou, and R. B. Liu for discussions. This work was supported by the Research Grant Council of Hong Kong under the Grant No.: HKU 7041/07P.

TABLE III: Comparison between charge sensing technique and spin sensing technique in the present work.

	Charge sensing ^{2,3}	Our model
Configuration		
Quantity manipulated and detected (Range)	Electron number in QD (0,1,2...)	Single spin in QD1 (-0.5 ~ 0.5)
Manipulation approach	Tuning gate voltage of QD	Applying large spin bias to QD1
Interaction between detector and detected	Coulomb repulsion	Exchange interaction $Js_1 \cdot s_2$
Detector	QPC	QD2
Measured quantity in detector	Charge conductance by applying charge bias	Spin conductance by applying spin bias

APPENDIX A: THE FORMULA OF SPIN CONDUCTANCE

The conventional zero-bias differential conductance for spin component σ is defined as

$$\mathcal{G}_\sigma^c = \lim_{V^c \rightarrow 0} \frac{\partial I_\sigma}{\partial V^c} = -\frac{e}{h} \lim_{V^c \rightarrow 0} \frac{\partial}{\partial V^c} \int d\omega (f_L - f_R) T_\sigma(\omega),$$

where without loss of generality the charge bias V^c is assumed to change only the Fermi level of the left lead,

$$f_L = \frac{1}{e^{(\omega - \mu + eV^c)/k_B T} + 1}, f_R = \frac{1}{e^{(\omega - \mu)/k_B T} + 1}, \quad (\text{A1})$$

and μ is the Fermi level of the both leads when there is no bias. Supposing the transmission probability T_σ is not a function of the bias,

$$\mathcal{G}_\sigma^c = -\frac{e}{h} \int d\omega \left[\frac{\partial f_L}{\partial V^c} \right]_{V^c \rightarrow 0} T_\sigma(\omega),$$

where $\left[\frac{\partial f_L}{\partial V^c} \right]_{V^c \rightarrow 0} \rightarrow -e\delta(\omega - \mu)$ when the temperature $k_B T \rightarrow 0$. So at zero temperature, the total conductance including two spin components

$$\mathcal{G}^c = \lim_{V^c \rightarrow 0} \frac{\partial (I_\uparrow + I_\downarrow)}{\partial V^c} = \sum_\sigma \mathcal{G}_\sigma^c = \frac{e^2}{h} [T_\uparrow(\mu) + T_\downarrow(\mu)].$$

If a spin bias V^s is applied so that $\mu_\uparrow^L = \mu_\downarrow^R = \mu - eV^s/2$ and $\mu_\downarrow^L = \mu_\uparrow^R = \mu + eV^s/2$, and at zero temperature

$$\begin{aligned} \left[\frac{\partial f_{L\uparrow}}{\partial V^s} \right]_{V^s \rightarrow 0} &= \left[\frac{\partial f_{R\downarrow}}{\partial V^s} \right]_{V^s \rightarrow 0} \rightarrow -\frac{e}{2} \delta(\omega - \mu), \\ \left[\frac{\partial f_{L\downarrow}}{\partial V^s} \right]_{V^s \rightarrow 0} &= \left[\frac{\partial f_{R\uparrow}}{\partial V^s} \right]_{V^s \rightarrow 0} \rightarrow \frac{e}{2} \delta(\omega - \mu). \end{aligned} \quad (\text{A2})$$

Then the differential conductance induced by the spin bias (or spin conductance for short) is defined as³¹

$$\mathcal{G}^s = \lim_{V^s \rightarrow 0} \frac{\partial (I_\uparrow + I_\downarrow)}{\partial V^s} = \frac{e^2}{h} [T_\uparrow(\mu) - T_\downarrow(\mu)], \quad (\text{A3})$$

which is proportional to difference between the transmission probabilities of two spin components. The physical picture of this definition is very clear. Because spin \uparrow and \downarrow are under opposite biases, I_\uparrow and I_\downarrow tend to flow along opposite directions. $|I_\uparrow|$ and $|I_\downarrow|$ must be unequal to generate net charge current, which is an experimentally measurable quantity. Notice that $|I_\uparrow|$ can be larger or smaller than $|I_\downarrow|$, depending on the ability of dot in conducting electron with spin \uparrow and \downarrow . Therefore the spin conductance can be either positive or negative. From Eq. (A3), one immediately realizes that if the spin symmetry of a mesoscopic system is broken, it can be probed by the spin conductance. Experimentally, one just applies a very small spin bias ΔV^s , then measures the net charge current ΔI (note that there is no need to measure the polarization of the current, instead the measurement of current direction is required), and performs $\Delta I / \Delta V^s$ to have an approximation of Eq. (A3).

APPENDIX B: DEDUCTION OF GREEN'S FUNCTIONS IN EQS. (8)

This part of calculation is inspired by the work by Tolea and Bulka,⁴⁵ in which an $\langle S^z \rangle = 0$ ($\langle s_1^z \rangle$ in our model) case was studied. Writing the equation of motion for $\langle\langle d_{2\uparrow} | d_{2\uparrow}^\dagger \rangle\rangle$ in the Fourier space

$$\begin{aligned} &(\omega - \epsilon_2 + \frac{i}{2}\Gamma_2) \langle\langle d_{2\uparrow} | d_{2\uparrow}^\dagger \rangle\rangle \\ &= 1 + \frac{J}{2} \langle\langle d_{2\downarrow} s_1^- | d_{2\uparrow}^\dagger \rangle\rangle + \frac{J}{2} \langle\langle d_{2\uparrow} s_1^z | d_{2\uparrow}^\dagger \rangle\rangle \\ &+ U_2 \langle\langle d_{2\uparrow} n_{2\downarrow} | d_{2\uparrow}^\dagger \rangle\rangle, \end{aligned} \quad (\text{B1})$$

where and in the following we suppress all the r superscript of the retarded Green's functions, and introduce the notation $\langle\langle A|B \rangle\rangle$ as the Fourier transform of $-i\theta(t) \langle\{A(t), B\}\rangle$. Continue writing the equation of motion of Green's functions that contain only operators $d_{2\sigma}$, $d_{2\sigma}^\dagger$ and $s_1^{z,\pm}$ until no more new Green's function is produced

$$\begin{aligned} &(\omega - \epsilon_2 + \frac{J}{4}) \langle\langle d_{2\downarrow} s_1^- | d_{2\uparrow}^\dagger \rangle\rangle \\ &= \frac{J}{4} \langle\langle d_{2\uparrow} | d_{2\uparrow}^\dagger \rangle\rangle - \frac{J}{2} \langle\langle d_{2\uparrow} s_1^z | d_{2\uparrow}^\dagger \rangle\rangle \\ &+ J \langle\langle d_{2\uparrow} n_{2\downarrow} s_1^z | d_{2\uparrow}^\dagger \rangle\rangle \\ &+ (\frac{J}{2} + U_2) \langle\langle d_{2\downarrow} n_{2\uparrow} s_1^- | d_{2\uparrow}^\dagger \rangle\rangle \\ &+ \sum_{k,\alpha} V_{k\alpha\downarrow} \langle\langle c_{k\alpha\downarrow} s_1^- | d_{2\uparrow}^\dagger \rangle\rangle, \end{aligned} \quad (\text{B2})$$

$$\begin{aligned} &(\omega - \epsilon_2) \langle\langle d_{2\uparrow} s_1^z | d_{2\uparrow}^\dagger \rangle\rangle \\ &= \langle s_1^z \rangle + \frac{J}{8} \langle\langle d_{2\uparrow} | d_{2\uparrow}^\dagger \rangle\rangle - \frac{J}{4} \langle\langle d_{2\downarrow} s_1^- | d_{2\uparrow}^\dagger \rangle\rangle \\ &+ \frac{J}{2} \langle\langle d_{2\downarrow} n_{2\uparrow} s_1^- | d_{2\uparrow}^\dagger \rangle\rangle + U_2 \langle\langle d_{2\uparrow} n_{2\downarrow} s_1^z | d_{2\uparrow}^\dagger \rangle\rangle \\ &+ \sum_{k,\alpha} V_{k\alpha\uparrow} \langle\langle c_{k\alpha\uparrow} s_1^z | d_{2\uparrow}^\dagger \rangle\rangle, \end{aligned} \quad (\text{B3})$$

$$\begin{aligned} &(\omega - \epsilon_2 - U_2) \langle\langle d_{2\uparrow} n_{2\downarrow} | d_{2\uparrow}^\dagger \rangle\rangle \\ &= \langle n_{2\downarrow} \rangle + \frac{J}{2} \langle\langle d_{2\downarrow} n_{2\uparrow} s_1^- | d_{2\uparrow}^\dagger \rangle\rangle + \frac{J}{2} \langle\langle d_{2\uparrow} n_{2\downarrow} s_1^z | d_{2\uparrow}^\dagger \rangle\rangle \\ &+ \sum_{k,\alpha} V_{k\alpha\downarrow} \langle\langle d_{2\uparrow} d_{2\downarrow}^\dagger c_{k\alpha\downarrow} | d_{2\uparrow}^\dagger \rangle\rangle \\ &- \sum_{k,\alpha} V_{k\alpha\downarrow} \langle\langle d_{2\uparrow} c_{k\alpha\downarrow}^\dagger d_{2\downarrow} | d_{2\uparrow}^\dagger \rangle\rangle \\ &+ \sum_{k,\alpha} V_{k\alpha\uparrow} \langle\langle c_{k\alpha\uparrow} n_{2\downarrow} | d_{2\uparrow}^\dagger \rangle\rangle, \end{aligned} \quad (\text{B4})$$

$$\begin{aligned}
& (\omega - \epsilon_2 - U_2) \langle \langle d_{2\uparrow} n_{2\downarrow} s_1^z | d_{2\uparrow}^\dagger \rangle \rangle \\
&= \langle n_{2\downarrow} s_1^z \rangle + \frac{J}{4} \langle \langle d_{2\downarrow} n_{2\uparrow} s_1^- | d_{2\uparrow}^\dagger \rangle \rangle + \frac{J}{8} \langle \langle d_{2\uparrow} n_{2\downarrow} | d_{2\uparrow}^\dagger \rangle \rangle \\
&+ \sum_{k,\alpha} V_{k\alpha\downarrow} \langle \langle d_{2\uparrow} d_{2\downarrow}^\dagger c_{k\alpha\downarrow} s_1^z | d_{2\uparrow}^\dagger \rangle \rangle \\
&- \sum_{k,\alpha} V_{k\alpha\downarrow} \langle \langle d_{2\uparrow} c_{k\alpha\downarrow}^\dagger d_{2\downarrow} s_1^z | d_{2\uparrow}^\dagger \rangle \rangle \\
&+ \sum_{k,\alpha} V_{k\alpha\uparrow} \langle \langle c_{k\alpha\uparrow} n_{2\downarrow} s_1^z | d_{2\uparrow}^\dagger \rangle \rangle, \tag{B5}
\end{aligned}$$

$$\begin{aligned}
& (\omega - \epsilon_2 - U_2 - \frac{J}{4}) \langle \langle d_{2\downarrow} n_{2\uparrow} s_1^- | d_{2\uparrow}^\dagger \rangle \rangle \\
&= -\langle d_{2\uparrow}^\dagger d_{2\downarrow} s_1^- \rangle + \frac{J}{4} \langle \langle d_{2\uparrow} n_{2\downarrow} | d_{2\uparrow}^\dagger \rangle \rangle \\
&+ \frac{J}{2} \langle \langle d_{2\uparrow} n_{2\downarrow} s_1^z | d_{2\uparrow}^\dagger \rangle \rangle \\
&- \sum_k V_{k\alpha\uparrow} \langle \langle d_{2\downarrow} c_{k\uparrow}^\dagger d_{2\uparrow} s_1^- | d_{2\uparrow}^\dagger \rangle \rangle \\
&+ \sum_k V_{k\alpha\uparrow} \langle \langle d_{2\downarrow} d_{2\uparrow}^\dagger c_{k\uparrow} s_1^- | d_{2\uparrow}^\dagger \rangle \rangle \\
&+ \sum_{k\alpha} V_{k\alpha\downarrow} \langle \langle c_{k\alpha\downarrow} n_{2\uparrow} s_1^- | d_{2\uparrow}^\dagger \rangle \rangle, \tag{B6}
\end{aligned}$$

where we have taken advantage of the singly-occupation of the dot 1, i.e. $n_{1\uparrow} + n_{1\downarrow} = 1$, so that

$$\begin{aligned}
s_1^{z/+} s_1^{+/-} &= \pm \frac{1}{2} s_2^+, \quad s_1^{z/-} s_1^{-/+} = \mp \frac{1}{2} s_2^-, \\
s_1^\pm s_1^\mp &= \frac{1}{2} \pm s_1^z, \quad (s_1^z)^2 = \frac{1}{4}. \tag{B7}
\end{aligned}$$

Using the approximation scheme proposed by the previous authors to treat quantum dots weakly coupled to

electrodes,^{45,46}

$$\begin{aligned}
\sum_{k\alpha} V_{k\alpha\uparrow} \langle \langle c_{k\alpha\uparrow} s_1^z | d_{2\uparrow}^\dagger \rangle \rangle &\approx -\frac{i}{2} \Gamma_2 \langle \langle d_{2\uparrow} s_1^z | d_{2\uparrow}^\dagger \rangle \rangle, \\
\sum_{k\alpha} V_{k\alpha\downarrow} \langle \langle c_{k\alpha\downarrow} s_1^- | d_{2\uparrow}^\dagger \rangle \rangle &\approx -\frac{i}{2} \Gamma_2 \langle \langle d_{2\downarrow} s_1^- | d_{2\uparrow}^\dagger \rangle \rangle, \\
\sum_{k\alpha} V_{k\alpha\uparrow} \langle \langle c_{k\alpha\uparrow} n_{2\downarrow} | d_{2\uparrow}^\dagger \rangle \rangle &\approx -\frac{i}{2} \Gamma_2 \langle \langle d_{2\uparrow} n_{2\downarrow} | d_{2\uparrow}^\dagger \rangle \rangle, \\
\sum_{k\alpha} V_{k\alpha\uparrow} \langle \langle c_{k\alpha\uparrow} n_{2\downarrow} s_1^z | d_{2\uparrow}^\dagger \rangle \rangle &\approx -\frac{i}{2} \Gamma_2 \langle \langle d_{2\uparrow} n_{2\downarrow} s_1^z | d_{2\uparrow}^\dagger \rangle \rangle, \\
\sum_{k\alpha} V_{k\alpha\downarrow} \langle \langle c_{k\alpha\downarrow} n_{2\uparrow} s_1^- | d_{2\uparrow}^\dagger \rangle \rangle &\approx -\frac{i}{2} \Gamma_2 \langle \langle d_{2\downarrow} n_{2\uparrow} s_1^- | d_{2\uparrow}^\dagger \rangle \rangle, \tag{B8}
\end{aligned}$$

where $\Gamma_2 = \Gamma_2^L + \Gamma_2^R$. Besides, simultaneously hopping in and out quantum dot are regarded as canceling with each other⁴⁶

$$\begin{aligned}
\langle \langle d_{2\uparrow} c_{k\alpha\downarrow}^\dagger d_{2\downarrow} | d_{2\uparrow}^\dagger \rangle \rangle &\approx \langle \langle d_{2\uparrow} d_{2\downarrow}^\dagger c_{k\alpha\downarrow} | d_{2\uparrow}^\dagger \rangle \rangle, \\
\langle \langle d_{2\uparrow} c_{k\alpha\downarrow}^\dagger d_{2\downarrow} s_1^z | d_{2\uparrow}^\dagger \rangle \rangle &\approx \langle \langle d_{2\uparrow} d_{2\downarrow}^\dagger c_{k\alpha\downarrow} s_1^z | d_{2\uparrow}^\dagger \rangle \rangle, \\
\langle \langle d_{2\downarrow} c_{k\alpha\uparrow}^\dagger d_{2\uparrow} s_1^- | d_{2\uparrow}^\dagger \rangle \rangle &\approx \langle \langle d_{2\downarrow} d_{2\uparrow}^\dagger c_{k\alpha\uparrow} s_1^- | d_{2\uparrow}^\dagger \rangle \rangle. \tag{B9}
\end{aligned}$$

The above approximations are valid only when the quantum dot is weakly coupled to the leads and for temperatures higher than the Kondo temperature. The advantage of the approximation is that it retains the full inter-dot correlations and gives a correct physical picture in Coulomb blockade regime. After applying the truncation approximation, the equation of motion for the spin \uparrow retarded Green's function of the dot 2 in the singly-occupied regime of the dot 1 can be obtained as Eqs. (8). The equation of motion for $\langle \langle d_{2\downarrow} | d_{2\downarrow}^\dagger \rangle \rangle$ can be obtained similarly.

* Electronic address: luhaizhou@gmail.com

¹ D. Loss and D. P. DiVincenzo, Phys. Rev. A **57**, 120 (1998).

² D. Sprinzak, Y. Ji, M. Heiblum, D. Mahalu, and H. Shtrikman, Phys. Rev. Lett. **88**, 176805 (2002).

³ J. M. Elzerman, R. Hanson, J. S. Greidanus, L. H. W. van Beveren, S. DeFranceschi, L. M. K. Vandersypen, S. Tarucha, and L. P. Kouwenhoven, Phys. Rev. B **67**, 161308(R) (2003).

⁴ R. Hanson, L. Kouwenhoven, J. R. Petta, S. Tarucha, and L. M. K. Vandersypen, Rev. Mod. Phys. (2007).

⁵ F. H. L. Koppens, C. Buizert, K.-J. Tielrooij, I. T. Vink, K. C. Nowack, T. Meunier, L. P. Kouwenhoven, and L. M. K. Vandersypen, Nature(London) **442**, 766 (2006).

⁶ K. C. Nowack, F. H. L. Koppens, Y. V. Nazarov, and L. M. K. Vandersypen, Science **318**, 1430 (2007).

⁷ J. M. Elzerman, R. Hanson, L. H. W. van Beveren, B. Witkamp, L. M. K. Vandersypen, and L. P. Kouwenhoven, Nature (London) **430**, 431 (2004).

⁸ R. Hanson, L. H. W. van Beveren, I. T. Vink, J. M. Elzerman, W. J. M. Naber, F. H. L. Koppens, L. P. Kouwenhoven, and L. M. K. Vandersypen, Phys. Rev. Lett. **94**, 196802 (2005).

⁹ I. Zutic, J. Fabian, and S. D. Sarma, Rev. Mod. Phys. **76**, 323 (2004).

¹⁰ M. Johnson and R. H. Silsbee, Phys. Rev. Lett. **55**, 1790 (1985).

¹¹ M. Johnson and R. H. Silsbee, Phys. Rev. Lett. **60**, 377 (1988).

¹² S. O. Valenzuela and M. Tinkham, Nature (London) **442**, 176 (2006).

¹³ A. T. Hanbicki, B. T. Jonker, G. Itskos, G. Kiioseoglou, and A. Petrou, Appl. Phys. Lett. **80**, 1240 (2002).

¹⁴ V. F. Motsnyi, J. D. Boeck, J. Das, W. V. Roy, G. Borghs, E. Goovaerts, and V. I. Safarov, Appl. Phys. Lett. **81**, 265 (2002).

¹⁵ H. J. Zhu, M. Ramsteiner, H. Kostial, M. Wassermeier, H. P. Schönher, and K. H. Ploog, Phys. Rev. Lett. **87**, 016601 (2001).

¹⁶ R. Fiederling, M. Keim, G. Reuscher, W. Ossau,

- G. Schmidt, A. Waag, and L. W. Molenkamp, *Nature (London)* **402**, 787 (1999).
- ¹⁷ Y. Ohno, D. K. Young, B. Beschoten, F. Matsukura, H. Ohno, and D. D. Awschalom, *Nature (London)* **402**, 790 (1999).
- ¹⁸ Y. Kato, R. C. Myers, A. C. Gossard, and D. D. Awschalom, *Science* **306**, 1910 (2004).
- ¹⁹ J. Wunderlich, B. Kaestner, J. Sinova, and T. Jungwirth, *Phys. Rev. Lett.* **94**, 047204 (2005).
- ²⁰ S. D. Ganichev, V. V. Bel'kov, S. A. Tarasenko, S. N. Danilov, S. Giglberger, C. Hoffmann, E. L. Ivchenko, D. Weiss, W. Wegscheider, C. Gerl, et al., *Nature Physics* **2**, 609 (2006).
- ²¹ X. D. Cui, S. Q. Shen, J. Li, Y. Ji, W. K. Ge, and F. C. Zhang, *Appl. Phys. Lett.* **90**, 242115 (2007).
- ²² J. Li, X. Dai, S.-Q. Shen, and F. C. Zhang, *Appl. Phys. Lett.* **88**, 162105 (2006).
- ²³ L. L. Sohn, L. P. Kouwenhoven, and G. Schön, eds., *Mesoscopic Electron Transport, NATO Advanced Study Institutes, Ser. E*, vol. 345 (Kluwer, Dordrecht, 1997).
- ²⁴ H. Park, J. Park, A. K. L. Lim, E. H. Anderson, A. P. Alivisatos, and P. L. McEuen, *Nature (London)* **407**, 57 (2000).
- ²⁵ Y. Chye, M. E. White, E. Johnston-Halperin, B. D. Gerardot, D. D. Awschalom, and P. M. Petroff, *Phys. Rev. B* **66**, 201301(R) (2002).
- ²⁶ J. Li and S.-Q. Shen, *Phys. Rev. B* **76**, 153302 (2007).
- ²⁷ M. Y. Veillette, C. Bena, and L. Balents, *Phys. Rev. B* **69**, 075319 (2004).
- ²⁸ P. Zhang, Q.-K. Xue, and X. C. Xie, *Phys. Rev. Lett.* **91**, 196602 (2003).
- ²⁹ Y. J. Bao, N. H. Tong, Q. F. Sun, and S. Q. Shen, unpublished.
- ³⁰ Q. F. Sun, X. Y. Xia, and S. Q. Shen, unpublished.
- ³¹ D.-K. Wang, Q. F. Sun, and H. Guo, *Phys. Rev. B* **69**, 205312 (2004).
- ³² P. W. Anderson, *Phys. Rev.* **124**, 41 (1961).
- ³³ H. Haug and A.-P. Jauho, *Quantum Kinetics in Transport and Optics of Semiconductors* (Springer-Verlag, Berlin Heidelberg, 1996).
- ³⁴ G. D. Mahan, *Many-Particle Physics* (Plenum Press, New York, 1990).
- ³⁵ J. C. Chen, A. M. Chang, and M. R. Melloch, *Phys. Rev. Lett.* **92**, 176801 (2004).
- ³⁶ M. Zaffalon and B. J. van Wees, *Phys. Rev. Lett.* **91**, 186601 (2003).
- ³⁷ P. Kotissek, M. Bailleul, M. Sperl, A. Spitzer, D. Schuh, W. Wegscheider, C. H. Back, and G. Bayreuther, *Nature Physics* **3**, 872 (2007).
- ³⁸ S. O. Valenzuela and M. Tinkham, *J. Appl. Phys.* **101**, 09B103 (2007), and references therein.
- ³⁹ A. W. Holleitner, C. R. Decker, H. Qin, K. Eberl, and R. H. Blick, *Phys. Rev. Lett.* **87**, 256802 (2001).
- ⁴⁰ I. H. Chan, R. M. Westervelt, K. D. Maranowski, and A. C. Gossard, *Appl. Phys. Lett.* **80**, 1818 (2002).
- ⁴¹ J. R. Petta, A. C. Johnson, J. M. Taylor, E. A. Laird, A. Yacoby, M. D. Lukin, C. M. Marcus, M. P. Hanson, and A. C. Gossard, *Science* **309**, 2180 (2005).
- ⁴² N. C. van der Vaart, S. F. Godijn, Y. V. Nazarov, C. J. P. M. Harmans, J. E. Mooij, L. W. Molenkamp, and C. T. Foxon, *Phys. Rev. Lett.* **74**, 4702 (1995).
- ⁴³ Q. F. Sun, H. Guo, and J. Wang, *Phys. Rev. Lett.* **90**, 258301 (2003).
- ⁴⁴ S. Datta, *Electronic Transport in Mesoscopic Systems* (Cambridge University Press, Cambridge, England, 1997).
- ⁴⁵ M. Tolea and B. R. Bulka, *Phys. Rev. B* **75**, 125301 (2007).
- ⁴⁶ B. R. Bulka and T. Kostyrko, *Phys. Rev. B* **70**, 205333 (2004).